JOURNAL OF MATERIALS SCIENCE 28 (1993) 2551–2556

# Evaluations of residual axial stresses and interfacial friction in Nicalon fibre-reinforced macro-defect-free cement composites

C. H. HSUEH, M. K. FERBER
*Metals and Ceramics Division, Oak Ridge National Laboratory Oak Ridge, TN 37831, USA*

The residual axial stress and the interfacial frictional stress of Nicalon fibre-reinforced macro-defect-free cement composites have been evaluated using the indentation technique. In these composites, both the residual axial stress in the fibre and the interfacial bonding are relatively high compared to other ceramic composites. Owing to the high residual axial stress, Poisson's effect can be ignored in analysing the stress–displacement relation of the fibre, and the interfacial frictional stress along the sliding length can be assumed to be a constant during indentation loading and unloading. Because of the strong interfacial bonding, consideration of the upper bound of the sliding zone length during unloading is essential. The sliding zone length during unloading is limited by the debond length at peak loading. The theoretical predictions of stress–displacement relations are in excellent agreement with the experimental results.

## 1. Introduction

The interfacial properties of fibre-reinforced composites can be evaluated by using the indentation technique [1–4]. Accurate evaluation of the interfacial properties requires detailed stress analyses of the stress–displacement relation of the fibre during the indentation loading and unloading processes. In the presence of Poisson's effect of the fibre (i.e. a non-uniform interfacial frictional stress along the sliding length), the stress analyses are formidable [2]. However, Poisson's effect can be ignored when the ratio of the peak loading stress to the residual axial stress in the fibre is sufficiently low [5], and simple analytical solutions for the stress–displacement relations are then attainable [5, 6]. Nicalon fibre-reinforced macro-defect-free (MDF) cement composites have a relatively high residual (compressive) axial stress in the fibre due to the high curing strain ( $\sim$ 20%) of the cement [4, 7]. Consequently, the residual axial stress and the interfacial friction of the Nicalon/MDF cement composite can be evaluated by ignoring Poisson's effect and assuming a constant frictional stress along the sliding length.

An analysis that ignores Poisson's effect but is used to evaluate identation data to obtain the residual axial stress has been established [6]. In the presence of the interfacial bonding, analytical solutions for the stress–displacement relation have also been obtained [6]. However, the solutions given by Marshall and Oliver [6] are limited to a condition where the loading stress required to initiate debonding (i.e. $\sigma_d$) is less than half of the peak loading stress (i.e. $\sigma^*$). When the above condition is not satisfied, modification of the analysis is required. This modification results from the fact that the sliding zone length during unloading is limited by the maximum debond length at peak loading [8]. Without this modification, an erroneous result will be obtained such that the sliding zone length during unloading is greater than the maximum debond length when $\sigma_d > \sigma^*/2$.

The purpose of the present study was to evaluate the residual axial stress and the interfacial frictional stress for Nicalon/MDF cement composites, a system in which both the residual axial stress and interfacial bonding are higher than other ceramic composites. In this paper, first, ignoring Poisson's effect, general solutions of the stress–displacement relations are derived. Then, neglect of Poisson's effect for the Nicalon/MDF cement composite is justified. Finally, the interfacial properties of Nicalon/MDF cement composites are evaluated, and the predicted stress–displacement relations are compared to the experimental results.

## 2. Analyses of stress–displacement relations

The indentation technique is shown schematically in Fig 1a. An indentor is used to push on the exposed end of an embedded fibre along the axial direction of the fibre, and forward sliding occurs at the fibre-matrix interface. The compressive loading stress, $\sigma$, increases during loading to a desired peak value, $\sigma^*$, and then decreases during unloading. Interfacial debonding and sliding initiate at $\sigma = \sigma_d$ during loading, and reverse sliding occurs during unloading. The stress–displacement relation at the exposed end of the fibre is recorded during the indentation loading and unloading processes (Fig. 1b). At the peak loading

0022–2461  

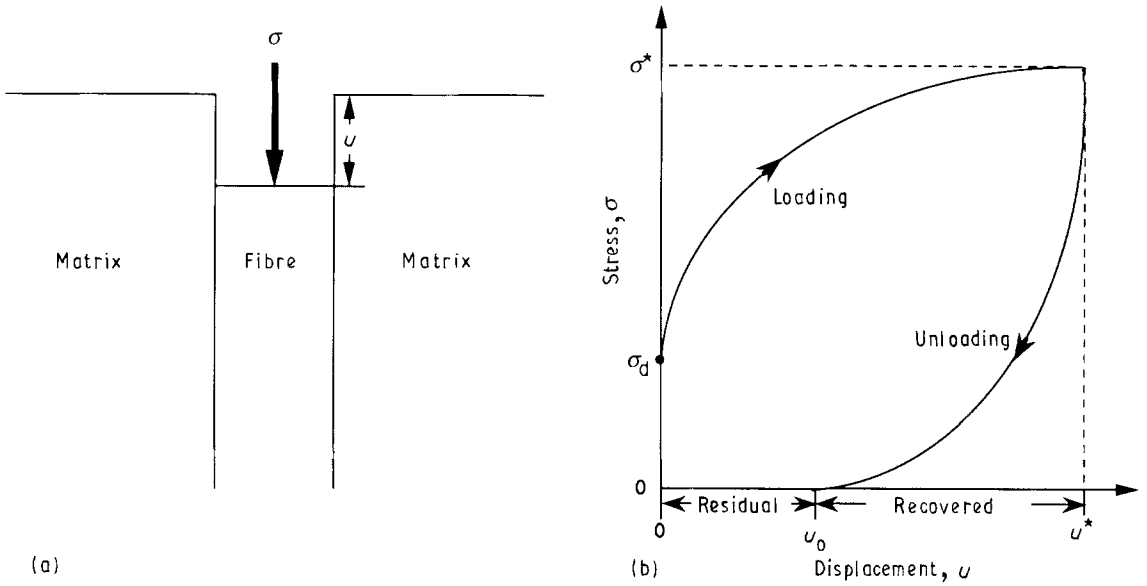


*Figure 1* Schematic diagrams of (a) indentation loading showing sliding at the fibre matrix interface and the axial displacement, $u$, at the exposed end of the embedded fibre, and (b) stress–displacement relation at the exposed end of the embedded fibre during loading and unloading.

stress, the corresponding fibre displacement is $u^*$. After complete unloading, the fibre displacement is $u_0$.

It has been shown in a previous study [5] that Poisson's effect and residual axial stress are two competitive factors that dictate the stress–displacement relation. Poisson's effect becomes more important when the peak loading stress to the interfacial residual clamping stress ratio increases. The effect of the residual axial stress becomes more important when the peak loading stress to the residual axial stress ratio decreases.

Nicalon/MDF cement composites have both a strong residual axial stress and strong interfacial bonding. Indentation on the Nicalon fibre shows that a significant loading stress, $\sigma_d$, is required to initiate interfacial debonding and sliding. Also, it will be shown in Section 3 that the stress–displacement behaviour of the fibre in the present indentation experiment is dominated by the residual axial stress. Hence, the present analyses are based on two conditions: (1) the interface remains bonded prior to external loading, and (2) Poisson's effect is negligible and the interfacial frictional stress is constant. It is noted that the conventional sign for a compressive stress is negative. The loading stress, $\sigma$, the debond stress, $\sigma_d$, and the residual axial stress, $\sigma_z$, are all compressive in the present study. However, to facilitate comparison between stresses, the negative sign is neglected and only the magnitudes of the stresses are considered.

## 2.1. Before loading (the residual compressive axial strain)

The fibre has a free surface, and the residual compressive axial strain, $\varepsilon$, is zero at $z = 0$. When interfacial bonding is sufficiently weak, interfacial debonding and sliding can occur due to the residual axial stress, and $\varepsilon$ increases linearly along the debonded interface to a constant, $\varepsilon_z$ ( $= \sigma_z/E_f$, see Fig. 2a), with the slope given by [1–6]

$$\frac{d\varepsilon}{dz} = -\frac{2\tau_i}{aE_f} \quad (1)$$

where $z$ is the axial coordinate, $a$ and $E_f$ are the radius and Young's modulus of the fibre, respectively, and $\tau_i$ is the constant interfacial frictional stress. When the interface is sufficiently strong, it can remain bonded. In this case, $\varepsilon$ increases quickly and reaches $\varepsilon_z$ within a length of a few fibre radii [9, 10] (see Fig. 2b). However, to simplify the present analysis, the residual axial strain, $\varepsilon$, is assumed to be constant and equals $\varepsilon_z$ along the entire fibre length when the interface remains bonded (see Fig. 2b).

## 2.2. Loading

The schematic diagram of the axial strain distribution of the fibre, $\varepsilon$, during loading is shown in Fig. 3. Interfacial debonding and sliding occur when the loading stress, $\sigma$, is greater than $\sigma_d$. The axial stress in the fibre is equal to $\sigma_d$ at the end of the debond length. Within the debond length, the slope of the curve is dictated by the stress transfer equation (Equation 1). The debond length, $t$, satisfying the above conditions is

$$t = \frac{a(\sigma - \sigma_d)}{2\tau_i} \quad (2)$$

The axial displacement (at the exposed end) of the fibre, $u$, is represented by the shaded area in Fig. 3, such that

$$u = \frac{a}{4E_f\tau_i}[\sigma^2 - \sigma_d^2 - 2\sigma_z(\sigma - \sigma_d)] \quad (3)$$

At the peak loading stress, $\sigma^*$, the debond length, $t^*$, is

$$t^* = \frac{a(\sigma^* - \sigma_d)}{2\tau_i} \quad (4)$$

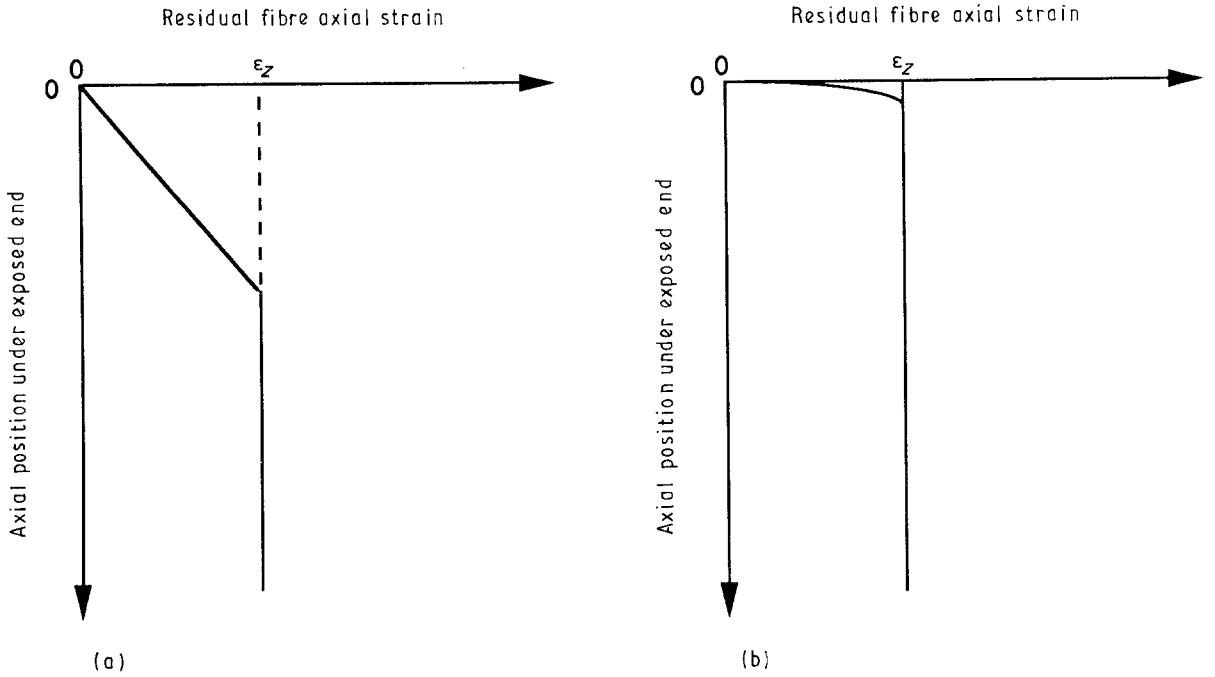


*Figure 2* Schematic representation of the residual axial strain distribution in the fibre, $\varepsilon$, for (a) a debonded interface, and (b) a bonded interface, where $\varepsilon_z$ is the equilibrium residual axial strain ( $= \sigma_z/E_f$).

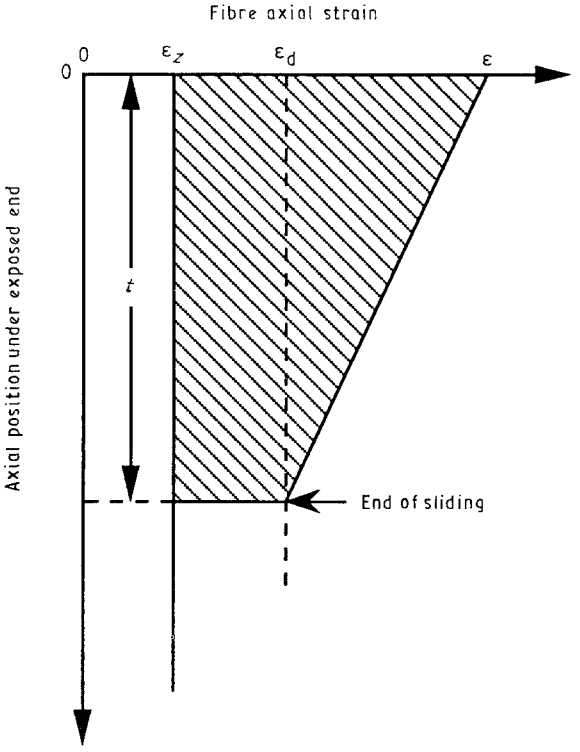


*Figure 3* Schematic representation of the axial strain distribution in the fibre during loading where $\varepsilon_d = \sigma_d/E_f > \varepsilon_z$ and $\varepsilon = \sigma/E_f$. The axial displacement at the exposed end of the fibre is represented by the shaded area.

The corresponding axial displacement of the fibre, $u^*$, is

$$u^* = \frac{a}{4E_f\tau_i}[\sigma^{*2} - \sigma_d^2 - 2\sigma_z(\sigma^* - \sigma_d)] \quad (5)$$

The stress–displacement relation has also been derived elsewhere [6] by calculating the energy change with interfacial crack extension. Instead of using the interfacial debond stress, $\sigma_d$, the interfacial fracture energy, $\gamma$, is adopted in the stress–displacement relation in [6]. However, relating $\gamma$ to $\sigma_d$, by using the relation in which the debond length is zero when the loading stress equals $\sigma_d$, the stress–displacement relation (for loading) obtained by Marshall and Oliver [6] becomes identical to the present result (Equation 3). Because $\sigma_d$ can be readily obtained from the experimental stress–displacement curve, the present results are more tractable. The debond stress, $\sigma_d$, can be related to either the interfacial fracture energy or the interfacial shear strength depending upon whether the energy-based [8, 11, 12] or the strength-based [13, 14] debonding criterion is adopted.

## 2.3. Unloading

During unloading, reverse sliding occurs starting at the surface and extending underneath the surface. This reverse sliding occurs at the already debonded interface, which is induced by the peak loading stress. Hence, the length for which the reverse sliding can occur (i.e. the reverse sliding zone length) is limited by $t^*$ (Equation 4). When $\sigma^* > 2\sigma_d$, the end of the reverse sliding zone length cannot reach the end of the maximum debond length (Fig. 4a). However, when $\sigma^* < 2\sigma_d$, the end of the reverse sliding zone length can reach the end of the maximum debond length (Fig. 4c). Hence, derivations of the stress–displacement relation require consideration of the following two cases.

### *2.3.1. The peak loading stress is greater than twice the debond stress*

When the applied stress is unloaded to $\sigma$, the axial stress in the fibre increases from $\sigma$ at the loaded end to $(\sigma + \sigma^*)/2$ at the end of the reverse sliding zone

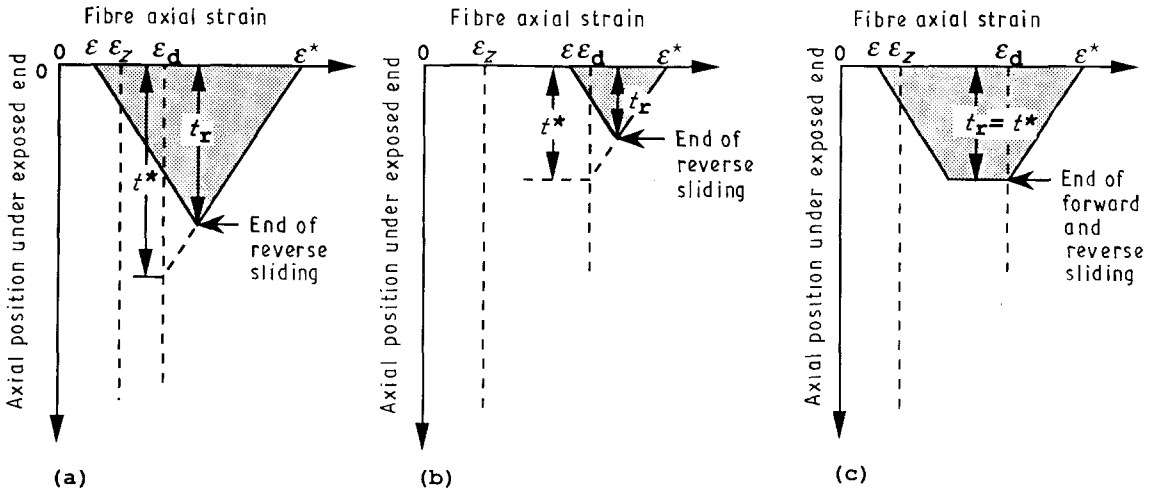


*Figure 4* Schematic representation of the axial strain distribution in the fibre during unloading for (a) $\varepsilon^* > 2\varepsilon_d$, (b) $\varepsilon^* < 2\varepsilon_d$ and $\varepsilon > 2\varepsilon_d - \varepsilon^*$, and (c) $\varepsilon^* < 2\varepsilon_d$ and $\varepsilon < 2\varepsilon_d - \varepsilon^*$. The recovered axial displacement at the exposed end of the fibre due to unloading is represented by the dotted area.

length (see Fig. 4a). The reverse sliding zone length, $t_r$, due to unloading is (Fig. 4a)

$$t_r = \frac{a(\sigma^* - \sigma)}{4\tau_i} \quad \text{for } \sigma^* > 2\sigma_d \tag{6}$$

The corresponding recovered axial displacement of the fibre, $u_r$, due to unloading is represented by the dotted area in Fig. 4a, such that

$$u_r = \frac{a(\sigma^* - \sigma)^2}{8E_f\tau_i} \quad \text{for } \sigma^* > 2\sigma_d \tag{7}$$

Hence, the net fibre displacement, $u\ (= u^* - u_r)$, for loading to $\sigma^*$ and then unloading to $\sigma$ is

$$u = \frac{a}{8E_f\tau_i}[\sigma^{*2} - \sigma^2 - 2\sigma_d^2 - 4\sigma_z(\sigma^* - \sigma_d) + 2\sigma^*\sigma] \quad \text{for } \sigma^* > 2\sigma_d \tag{8}$$

After complete unloading (i.e. $\sigma = 0$ in Equation 8), the residual fibre displacement, $u_0$, becomes

$$u_0 = \frac{a}{8E_f\tau_i}[\sigma^{*2} - 2\sigma_d^2 - 4\sigma_z(\sigma^* - \sigma_d)] \quad \text{for } \sigma^* > 2\sigma_d \tag{9}$$

The relative residual fibre displacement, $u_0/u^*$, is

$$\frac{u_0}{u^*} = \frac{\sigma^{*2} - 2\sigma_d^2 - 4\sigma_z(\sigma^* - \sigma_d)}{2[\sigma^{*2} - \sigma_d^2 - 2\sigma_z(\sigma^* - \sigma_d)]} \quad \text{for } \sigma^* > 2\sigma_d \tag{10}$$

### 2.3.2. The peak loading stress is less than twice the debond stress

When $\sigma^* < 2\sigma_d$ and $\sigma > 2\sigma_d - \sigma^*$, the reverse sliding zone is still confined by the maximum debonding zone, $t^*$ (Fig. 4b), and the analyses in Section 2.3.1 are valid, such that

$$t_r = \frac{a(\sigma^* - \sigma)}{4\tau_i} \quad \text{for } \sigma^* < 2\sigma_d \text{ and } \sigma > 2\sigma_d - \sigma^* \tag{11}$$

$$u = \frac{a}{8E_f\tau_i}[\sigma^{*2} - \sigma^2 - 2\sigma_d^2 - 4\sigma_z(\sigma^* - \sigma_d) + 2\sigma^*\sigma] \quad \text{for } \sigma^* < 2\sigma_d \text{ and } \sigma > 2\sigma_d - \sigma^* \tag{12}$$

When $\sigma^* < 2\sigma_d$ and $\sigma < 2\sigma_d - \sigma^*$, the end of the reverse sliding zone length reaches the end of the maximum debond length (Fig. 4c). The reverse sliding zone length, $t_r$, is limited by $t^*$, such that

$$t_r = t^* \quad \text{for } \sigma^* < 2\sigma_d \text{ and } \sigma < 2\sigma_d - \sigma^* \tag{13}$$

The axial stress is the fibre increases from $\sigma$ at the loaded end to $\sigma + \sigma^* - \sigma_d$ at the end of the reverse sliding zone length. The corresponding recovered axial displacement of the fibre, $u_r$, due to unloading is represented by the dotted area in Fig. 4c, such that

$$u_r = \frac{a(\sigma^* - \sigma_d)(\sigma_d - \sigma)}{2E_f\tau_i} \quad \text{for } \sigma^* < 2\sigma_d \text{ and } \sigma < 2\sigma_d - \sigma^* \tag{14}$$

The net fibre displacement, $u\ (= u^* - u_r)$, is

$$u = \frac{a}{4E_f\tau_i}[(\sigma^* - \sigma_d)(\sigma^* - \sigma_d - 2\sigma_z + 2\sigma)] \quad \text{for } \sigma^* < 2\sigma_d \text{ and } \sigma < 2\sigma_d - \sigma^* \tag{15}$$

After complete unloading (i.e. $\sigma = 0$ in Equation (15), the residual fibre displacement, $u_0$, becomes

$$u_0 = \frac{a}{4E_f\tau_i}[(\sigma^* - \sigma_d)(\sigma^* - \sigma_d - 2\sigma_z)] \quad \text{for } \sigma^* < 2\sigma_d \tag{16}$$

The relative residual fibre displacement, $u_0/u^*$, is

$$\frac{u_0}{u^*} = \frac{(\sigma^* - \sigma_d)(\sigma^* - \sigma_d - 2\sigma_z)}{\sigma^{*2} - \sigma_d^2 - 2\sigma_z(\sigma^* - \sigma_d)} \quad \text{for } \sigma^* < 2\sigma_d \tag{17}$$

### 2.4. $u_0/u^*$ versus $\sigma_d/\sigma^*$ relations

The calculated $u_0/u^*$ versus $\sigma_d/\sigma^*$ relations are shown in Fig. 5 at different values of $\sigma_z/\sigma^*$ for $\sigma_d > 2\sigma_z$, such that the interface remains bonded before loading [8]. The $u_0/u^*$ versus $\sigma_d/\sigma^*$ relations are dictated by Equations 10 and 17 when $\sigma_d/\sigma^* < 0.5$ and $\sigma_d/\sigma^* > 0.5$, respectively, and are represented by the solid lines in Fig. 5. However, without the modification for the case of $\sigma_d/\sigma^* > 0.5$, the erroneous results (i.e. when the $u_0/u^*$ versus $\sigma_d/\sigma^*$ relation is dictated by Equation 10 for $\sigma_d/\sigma^* > 0.5$) are shown by the broken lines in Fig. 5. These errors increase when the positive deviation of $\sigma_d/\sigma^*$ from 0.5 increases.

## 3. Residual axial stress versus Poisson's effect for Nicalon/MDF cement composites

It has been shown that ignoring the residual axial stress, Poisson's effect and interfacial bonding, the relative residual fibre displacement, $u_0/u^*$, is 0.5 [1, 2, 5]. The presence of the compressive residual axial stress (in the fibre), Poisson's effect, or interfacial bonding can contribute to the negative deviation of $u_0/u^*$ from 0.5 [2, 5]. Poisson's effect and residual axial stress are two competitive factors in dictating the stress–displacement relation. When the applied stress is less than a critical value, Poisson's effect can be ignored in analysing the stress–displacement relation [5]. In this section we find this critical applied stress, and justify that Poisson's effect can be ignored for Nicalon/MDF cement composites.

For the purpose of comparing the role of the residual axial stress to that of Poisson's effect on the deviation of $u_0/u^*$ from 0.5, interfacial bonding is ignored in this section. The prediction of $u_0/u^*$ from the analysis considering the residual axial stress is contingent upon the determination of the residual compressive axial stress, $\sigma_z$, in the fibre [5]. For Nicalon/MDF cement composites ($E_f = 200$ GPa, $E_m = 80$ GPa, $\nu_f = 0.15$, $\nu_m = 0.2$, and $a = 8.5$ μm), it will be shown in Section 4 that $\sigma_z$ is about 129 MPa and the interfacial frictional stress, $\tau_i$, is about 13 MPa. The prediction of $u_0/u^*$ from the analysis considering Poisson's effect is contingent upon the determination of the residual clamping stress, $\sigma_c$, and the coefficient of friction, $\mu$, at the interface [5]. These two parameters, $\sigma_c$ and $\mu$, can be evaluated from $\sigma_z$ and $\tau_i$ as shown below.

When the residual stress is due to an isotropic mismatch strain between the fibre and the matrix, the interfacial clamping stress, $\sigma_c$, can be related to $\sigma_z$ by [5, 15]

$$\sigma_z = \left[1 + \frac{(1+\nu_m)E_f}{(1+\nu_f)E_m}\right]\sigma_c \qquad (18)$$

where $E$ and $\nu$ are Young's modulus and Poisson's ratio, and the subscripts f and m denote the fibre and the matrix, respectively. The interfacial clamping stress, $\sigma_c$, calculated from Equation 18, is 35.7 MPa, and the coefficient of friction, $\mu$, calculated from $\tau_i = \mu\sigma_c$ is 0.36.

Ignoring interfacial bonding, the predicted $u_0/u^*$ versus $\sigma^*$ relations for considering either Poisson's effect or residual axial stress are shown in Fig. 6 based on the analysis given elsewhere [5] and the above material properties. The residual axial stress dominates the deviation of $u_0/u^*$ from 0.5 when the peak loading stress is less than about 1.8 GPa, which is satisfied by the general loading condition. Hence, Poisson's effect for these particular Nicalon/MDF cement composites can be ignored.

## 4. Evaluations of residual axial stress and interfacial bonding for Nicalon/MDF cement composites

Nicalon fibres are coated with silane prior to processing the composite, and the detailed processes have been described earlier [4]. The experimental stress–displacement relation for Nicalon/MDF cement composites during loading and unloading is shown in Fig. 7 at peak compressive loading stresses of $\sigma^* = 403.2$ MPa. The fibre protrudes above the matrix after complete unloading which is signified by

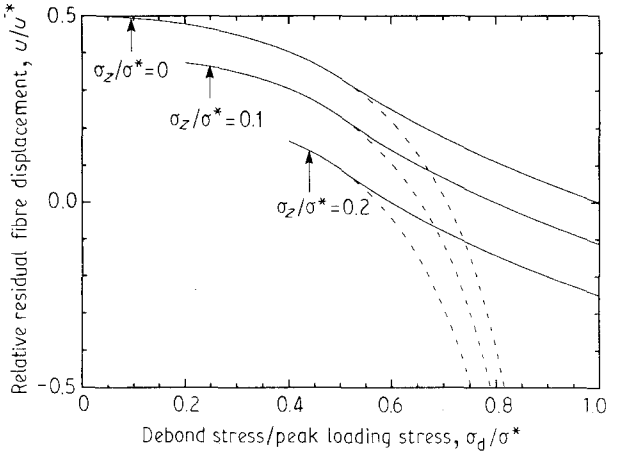


*Figure 5* The $u_0/u^*$ versus $\sigma_d/\sigma^*$ relations at different values of $\sigma_z/\sigma^*$ for $\sigma_d > \sigma_z$. (——) Modified correct predictions, ( - - - ) the erroneous predictions.

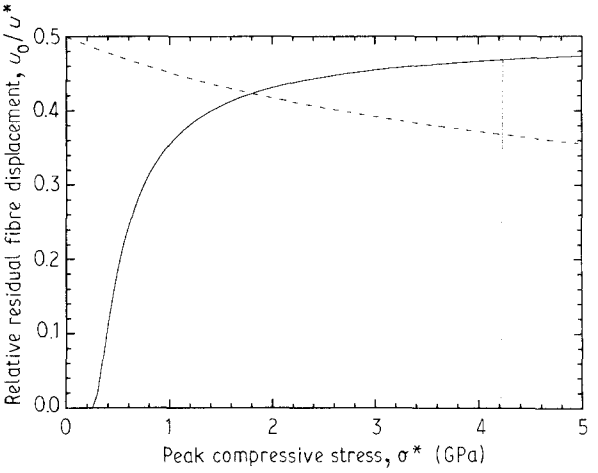


*Figure 6* The relative residual fibre displacements after indentation loading and unloading, $u_0/u^*$, as functions of the peak compressive loading stress, $\sigma^*$. ( - - - ) Poisson's effect consideration, (— —) residual axial stress consideration for Nicalon/MDF cement composites.

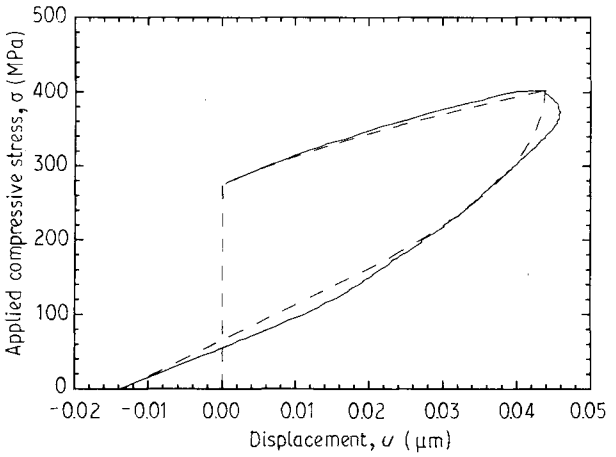


*Figure 7* The load–displacement ($\sigma$–$u$) relation of the Nicalon fibre in the Nicalon/MDF cement composite for $\sigma^* = 403.2$ MPa ($< 2\sigma_d$). (——) Experimental results, (– – –) theoretical predictions. $u_0/u^* = -0.31$, $\sigma_z = -129$ MPa, $\tau_i = 13$ MPa.

the negative value of $u_0/u^*$ in Fig. 7. The debond stress, $\sigma_d$, obtained from Fig. 7 is 276 MPa. The loading condition in Fig. 7 satisfies $\sigma^* < 2\sigma_d$. The steps in evaluating the residual axial stress and the interfacial frictional stress are summarized as follows. First, the experimental value of $u_0/u^*$ is obtained. Then, the residual axial stress is calculated from this $u_0/u^*$ value ($= -0.31$) and Equations 10 and 17, such that

$$\sigma_z = \frac{\left[\sigma^{*2} - 2\sigma_d^2 - \frac{2u_0}{u^*}(\sigma^{*2} - \sigma_d^2)\right]}{4\left(1 - \frac{u_0}{u^*}\right)(\sigma^* - \sigma_d)}$$

$$\text{for } \sigma^* > 2\sigma_d \tag{19a}$$

$$\sigma_z = \frac{\left[\sigma^* - \sigma_d - \frac{u_0}{u^*}(\sigma^* - \sigma_d)\right]}{2\left(1 - \frac{u_0}{u^*}\right)}$$

$$\text{for } \sigma^* < 2\sigma_d \tag{19b}$$

Finally, the interfacial frictional stress, $\tau_i$, is obtained by comparing the predicted to the experimental $\sigma$–$u$ curves.

The calculated $\sigma$–$u$ curve is also shown in Fig. 7 (where $\sigma_z = 129$ MPa and $\tau_i = 13$ MPa), and excellent agreement between predicted and experimental $\sigma$–$u$ curves is obtained. The deviation between the predicted and the experimental unloading curves occurring near the peak load is due to the measurement error in the experimental data. This error results from hysteresis effects in the indentation load train, which arises during load reversal. Normally, the hysteresis error is a relatively small component of the fibre sliding displacement. However, in the case of Nicalon/MDF system, fibre sliding is quite limited such that the hysteresis during load reversal has a measurable effect on the stress–displacement unloading curve.

## 5. Conclusion

In evaluating the interfacial properties of fibre-reinforced composites by using the indentation technique, Poisson's effect can be ignored when the ratio of the peak loading stress to the residual axial stress in the fibre is sufficiently low. Ignoring Poisson's effect, the stress–displacement relation during loading and unloading has been analysed [6]. However, the existing solution [6] is limited to the case where the peak loading stress, $\sigma^*$, is greater than twice the debond stress, $\sigma_d$. The present study provides the general solutions. These solutions are then applied to evaluate the interfacial properties of Nicalon/macro-defect-free cement composites, which have both a strong residual axial stress and strong interfacial bonding. The indentation technique has been performed on Nicalon/MDF cement composites for $\sigma^* < 2\sigma_d$ (see Fig. 7). Excellent agreement between the predicted and the experimental stress–displacement relations was obtained.

## Acknowledgement

We thank Drs P. F. Becher, J. H. Schneibel and H. T. Lin for reviewing the manuscript. This research was jointly sponsored by the US Department of Energy, Division of Materials Sciences, and the Assistant Secretary for Conservation and Renewable Energy, Office of Industrial Technologies, Industrial Energy Efficiency Division, under contract DE-AC05-84OR21400 with Martin Marietta Energy Systems, Inc.

## References

1. D. B. MARSHALL and W. C. OLIVER, *J. Amer. Ceram. Soc.* **70** (1987) 542.
2. C. H. HSUEH, M. K. FERBER and P. F. BECHER, *J. Mater. Res.* **4** (1989) 1529.
3. T. P. WEIHS and W. D. NIX, *J. Amer. Ceram. Soc.* **74** (1991) 524.
4. M. K. FERBER, A. A. WERESZCZAK, D. H. HANSEN and J. HOMENY, *Compos. Sci. Technol.*, in press
5. C. H. HSUEH, M. K. FERBER and A. A. WERESZCZAK, *J. Mater. Sci.*, **28** (1993) 2227.
6. D. B. MARSHALL and W. C. OLIVER, *Mater. Sci. Engng* **A126** (1990) 95.
7. N. McN. ALFORD and J. D. BIRCHALL, *Mater. Res. Soc. Symp. Proc.* **42** (1985) 265.
8. D. B. MARSHALL, *Acta Metall. Mater.* **40** (1992) 427.
9. L. N. McCARTNEY, *Proc. Roy. Soc. Lond.* **A425** (1989) 215.
10. C. H. HSUEH, *Mater. Sci. Engng* **A145** (1991) 135.
11. C. GURNEY and J. HUNT, *Proc. Roy. Soc. Lond.* **A299** (1967) 508.
12. H. STANG and S. P. SHAH, *J. Mater. Sci.* **21** (1986) 953.
13. A. TAKAKU and R. G. C. ARRIDGE, *J. Phys. D Appl. Phys.* **6** (1973) 2038.
14. C. H. HSUEH, *Mater. Sci. Engng* **A123** (1990) 1.
15. C. H. HSUEH, P. F. BECHER and P. ANGELINI, *J. Amer. Ceram. Soc.* **71** (1988) 929.

*Received 7 July*
*and accepted 19 October 1992*